Journal of Materials Chemistry A

Accepted Manuscript

ROYAL SOCIETY OF CHEMISTRY

www.rsc.org/materialsA

Journal Name

ARTICLE

Received 00th January 20xx,

Accepted 00th January 20xx

DOI: 10.1039/x0xx00000x

www.rsc.org/

Porous $NiCo_2O_4$ nanotubes as noble metal-free effective bifunctional catalysts for rechargeable Li–O_2 batteries

Laiyang Li,[a] Laifa Shen,[a] Ping Nie,[a] Gang Pang,[b] Jie Wang,[a] Hongsen Li,[a] Shengyang Dong,[a] and Xiaogang Zhang*[a]

Porous $NiCo_2O_4$ nanotubes have been successfully synthesized by a facile and cost-effective electrospinning method as noble metal-free catalysts for rechargeable Li–O_2 batteries. The as-synthesized $NiCo_2O_4$ nanotubes with hollow cavity and porous wall is found to superiorly improve the electrochemical performance of the Li–O_2 batteries, including a high initial discharge capacity, reduced overpotential as well as good rate capability. Excellent cycling stability over 110 cycles with the highly discharged voltage platform of 2.4 V at 200 mA g_c^{-1} was achieved. By means of the FESEM, XRD, Raman spectroscopy and GITT analysis, the toroidal-shaped Li_2O_2 particles were identified as the dominant discharge product and revealed the Li_2O_2 can be completely decomposed during the charge process, indicating its superior reversibility as effective bifunctional catalysts for Li–O_2 batteries. All the results indicated that the porous $NiCo_2O_4$ nanotubes expressed intriguing properties and great potential applications as noble metal-free effective bifunctional catalysts for rechargeable Li–O_2 batteries.

Introduction

In search for high−efficiency energy storage devices, rechargeable nonaqueous Li−O_2 batteries are extremely attractive due to the high theoretical gravimetric energy density of 11140 Wh kg^{-1}, which can meet the requirements for the long-range electric vehicles applications.[1–4] However, Li−O_2 batteries still face numerous challenges in their practical applications, including: (1) the horribly sluggish oxygen reduction reaction (ORR) and oxygen evolution reaction (OER) kinetics not only increase the overpotential but have influence on the overall performance of Li−O_2 batteries;[5–7] (2) the build-up of the insoluble discharge products (Li_2O_2) and the unavoidable formation of side products (Li_2CO_3) on the cathode would gradually obstruct the catalytic sites and the diffusion pathways of oxygen and electrolyte, leading to a detrimental overpotential.[8–10] Therefore, restricting the capacity, rate capability and cycling performances of the Li−O_2 batteries. In response, it is highly desirable to rationally explore an optimal cathode catalysts involving highly active, stable and porous structure to efficiently catalyze ORR and OER as well as facilitating rapid diffusion of O_2 and electrolyte, which would improve the round-trip efficiency, capacity and cycling stability performance of the Li−O_2 batteries.[11–14] Although Au,[15] Pt,[16] Pd,[8] and Ru,[17, 18] based noble metals materials exhibited superior catalytic properties for ORR or OER, the preciousness and scarcity have limited their widespread applications for the Li−O_2 batteries. Non-precious catalysts have attracted special attention, such as carbon materials and transition metal oxides with high catalytic activities, natural abundance and relatively low cost. Unfortunately, carbon materials are unstable in reaction with discharge products, oxidatively decomposing to form Li_2CO_3, which further promote electrolyte decomposition and lead to a higher overpotential and poor cycle stability during discharge and charge in Li−O_2 batteries.[19–24]

Transition metal oxides such as MnO_2,[25] Co_3O_4,[26, 27] Mn_3O_4,[28] Fe_3O_4,[29] and $CoMn_2O_4$,[30, 31] have been extensively explored as cathode catalysts for metal-air batteries owning to their low cost, abundance and high catalytic abilities for ORR and OER. In particular, Co_3O_4 has attracted much attention in electrocatalytic activity for the Li−O_2 batteries due to its intriguing electrochemical properties.[26, 27, 32, 33] Cobalt is poisonous and expensive, it is thus desirable to substitute Co with environmentally friendly and cheaper alternative element to enhance its electrochemical properties.[34, 35] Excitingly, spinel nickel cobaltice ($NiCo_2O_4$) has been extensively investigated as electrode materials for energy storage devices including supercapacitors and lithium-ion batteries (LIBs), due to possessing much higher electrical conductivity than cobalt oxides or nickel oxides.[36, 37] Furthermore, $NiCo_2O_4$ has been recently investigated as efficient bifunctional catalytic toward ORR and OER for the Li–O_2 batteries. Various different types of $NiCo_2O_4$ nanostructures, including nanoflakes,[38] nanosheets,[39] nanorods,[40] nanowires,[41] and microspheres,[42] have been synthesized and their efficient cathode catalysts for the Li–O_2 batteries were intensively investigated. Sun et al. reported the synthesis of $NiCo_2O_4$ nanorods by a hydrothermal method and exhibited a superior catalytic activity

[a] Jiangsu Key Laboratory of Materials and Technology for Energy Conversion, College of Materials Science and Engineering， Nanjing University of Aeronautics and Astronautics Nanjing, 210016, P. R. China. E-mail: azhangxg@nuaa.edu.cn Fax: +86 025 52112626; Tel: +86 025 52112902

[b] School of Materials Science and Engineering, Anhui University of Technology, Maanshan, 243002, P. R. China.

† Electronic Supplementary Information (ESI) available: [details of any supplementary information available should be included here]. See DOI: 10.1039/x0xx00000x

in rechargeable Li–O_2 batteries.[40] Lu et al. successfully synthesized a hierarchical $NiCo_2O_4$ spinel nanowire array by a facile co-precipitation method , which showed an improved cyclability for 50 cycles with a limited capacity of 1000 mAh g^{-1}.[41] Porous MCo_2O_4 (M = Mn, Fe, Ni, and Zn) nanorods were also prepared through a simple hydrothermal reaction and used as cathode catalysts for Li−O_2 batteries.[43] The porous $NiCo_2O_4$ nanorods electrode delivered the discharging overpotential of 1.53 V and the cyclability of 40 cycles with a cutoff capacity of 500 mAh g^{-1}. Apparently, porous and hollow nanostructure catalysts expose much more catalytic active sites and possess better catalytic properties in comparison with their solid structure, because oxygen and electrolyte can effectively diffuse into the hollow cavities of porous nanotubes. As far as we known, limited investigations have been carried out on the application of the porous and hollow $NiCo_2O_4$ nanostructure as cathodic catalyst for the nonaqueous Li−O_2 batteries.

In this work, porous $NiCo_2O_4$ (NCO) nanotubes were successfully prepared by a facile electrospinning method. When used as the catalyst in Li−O_2 batteries, the one-dimensional (1D) porous nanotubes can effectively facilitate the electronic transport, the electrolyte diffusion and the O_2 breathing, while simultaneously provide a large contact area of electrode-electrolyte to assure high-efficiency availability of the catalytic reaction sites for O_2/Li_2O_2 conversion. Electrochemical measurements results show that the 1D porous NCO nanotubes superiorly improve the performance of the Li−O_2 batteries, giving a high initial discharge capacity, reduced overpotential, better rate capability and long cycle life.

Experimental Section

Materials synthesis

All chemical reagents were of analytical grade and were used as received. Typically, PVP (poly(vinylpyrolidone), M_w = 360 000 g mol^{-1}) was dissolved in a mixed of ethanol (5 mL) and DMF (N,N−dimethylformamide, 5 mL) solution with vigorous stirring to form a 10 wt% homogeneous solution. 0.7 mmol of $Ni(NO_3)_2{\cdot}6\ H_2O$ and 1.4 mmol $Co(NO_3)_2{\cdot}6\ H_2O$ were then added to the resulting solution. Subsequently, the mixture was vigorously stirred for 24 h at room temperature, and then a viscous and pink solution can be obtained. Then the precursor solution was loaded into a plastic syringe with a stainless steel nozzle, which was connected to a high−voltage power supply. The flow rate and an applied voltage between the needle tip and collector were 0.5 ml h^{-1} and 18 kV, respectively, the as-prepared solution was electrospun into nanofibers. Finally, the obtained as−spun fibers were calcinated at 450°C for 2 h in air.

Materials characterization

The crystal structure of the obtained samples was characterized by powder X−ray diffraction (XRD) (Bruker D8 advance) with Cu Kα radiation. The microstructural properties of the resultant samples were characterized using field-emission scanning electron microscopy (FESEM, HITACHI S−4800) and high-resolution transmission electron microscopy (TEM, JEOL JEM−2010). The N_2 adsorption-desorption were determined by BET measurements using an ASAP−2010 surface area analyzer. The Raman spectra of NCO/CB electrodes were measured by the Raman spectrometer system (HORIBA Scientific LabRAM HR) with a 532.4 nm diode laser at room temperature.

Li–O_2 Battery assembly and measurements

The O_2 catalytic electrodes were prepared by coating a homogeneous ink consisting of as-prepared $NiCo_2O_4$ nanotubes (40 wt%), carbon black (acetylene carbon black, 40 wt%), and a PVDF binder (20 wt%) mixture in N-methyl-2-pyrrolidinone (NMP), and the resulting slurry was coated onto a carbon paper (TGP-H-060 carbon paper, Torray). The total mass loading of the carbon was approximately 0.8 mg cm^{-2}. The coated electrode was dried for 12 h at 80 °C under vacuum to remove any residual solvent. The batteries were assembled in a glove box under an Ar atmosphere. A metallic lithium anode was separated by a glass microfibre separator (Whatman), soaked in 1 M LiTFSI in the TEGDME electrolyte. A Swagelok type cell with an air hole (0.8 cm^{-2}) on the cathode side was used to allow the oxygen to flow into. All the measurements are conducted in a 1 atm dry oxygen atmosphere to avoid any negative effects of humidity and CO_2. The galvanostatically charge/discharge performance was conducted by a LAND–CT2001A battery-testing instrument (Wuhan Land Electronic Co. Ltd.). The specific capacity and current density were based on the amount of carbon used into the catalysts. The cyclic voltammograms (CVs) with a scan rate of 0.1 mV s^{-1} were also performed in the range of 2.0–4.5 V at room temperature.

Results and discussion

The precursor nanofibers were prepared by a simple, facile and cost-effective electrospinning technique (see the experimental section). Then, the porous NCO nanotubes were obtained by calcinated at 450°C for 2 h in the air flow. The morphology and microstructure of the as-synthesized NCO materilas are examined with field-emission scanning electron microscopy (FESEM) and TEM. As shown in Fig. 1a, the as-electrospun nanofibers have a continuous and smooth surface with the diameters of ca. 250 nm. Intriguingly, after annealing in the air, a hollow nanotube structure is obtained (Fig. 1b and Fig. S1a). The diameter of the obtained NCO nanotubes decreases to about 100 nm and many small pores in the wall of nanotubes are formed. The general formation process of hollow porous nanotubes structure mainly includes two steps, electrospinning and thermal treatment procedure. In short, it has been found that the concentration of precursor solution and the rational control heating rate have an important effect on fabrication the hollow structures. Specifically, in the thermal treatment process, by using a relatively low heating rate, the as-electrospun nanofibers might act a structural template role for assuring the formation of hollow structures[37, 44, 45]. Meanwhile, the precursor nanofibers would be gradually removed, and homogeneously heated from the surface to the centre and Ostwald ripening process, which gives rise to the in situ develop the relatively rigid wall. Besides, the small pores on the surface of nanotubes might be due to the decomposition of precursor component and outward diffusion of generated gases

during the annealing process. The morphology and structure of porous NCO nanotubes are further elucidated by TEM. As shown in Fig. 1c and Fig. S1b, the porous NCO nanotubes with diameter of about 100 nm and small pores on the surface of nanotubes can be clearly observed, which are in accordance with the FESEM observation. Furthermore, TEM image depicted in Fig. 1c and Fig. S1b reveals that typical porous NCO nanotubes have the wall thickness about 25 nm and are composed of NCO nanocrystals with the size of 10−30 nm in diameter. A interplanar spacing of 0.468 nm is observed in the HRTEM image (Fig. 1d), which matches well with the (111) lattice planes of spinel NCO phase. The TEM elemental mapping of a single nanotube structure in Fig. 1e1-e4 further illustrates the successful synthesis of the hollow product, meanwhile indicates the homogeneous dispersion of Ni, Co and O elements in the hollow nanotube structures. In addition, the XRD pattern reveals that all the diffraction peaks of the product could be readily indexed to well-crystallized cubic spinel NCO phase (JCPDS card No. 20-0781; Fig. 2a), indicating high purity of the prepared sample. The N_2 adsorption–desorption isotherm (Fig. 2b) of the porous $NiCo_2O_4$ nanotubes displays the type IV curves with a surface area of 30.2 m^2 g^{-1}. From the pore-size distribution curve, it is clearly observed that the pore size in the range with size of ~3 to 30 nm confirms the mesoporous structure of the sample, which is in good agreement with the electron microscope results. The 1D hollow porous structure can effectively facilitate the electron transfer, the electrolyte impregnation and the O_2 breathing, while simultaneously provide a large contact area of electrode–electrolyte to assure high-efficiency availability of the catalytic sites for ORR and OER. All these advantages would contribute to improve the electrochemical performance of Li–O_2 batteries.

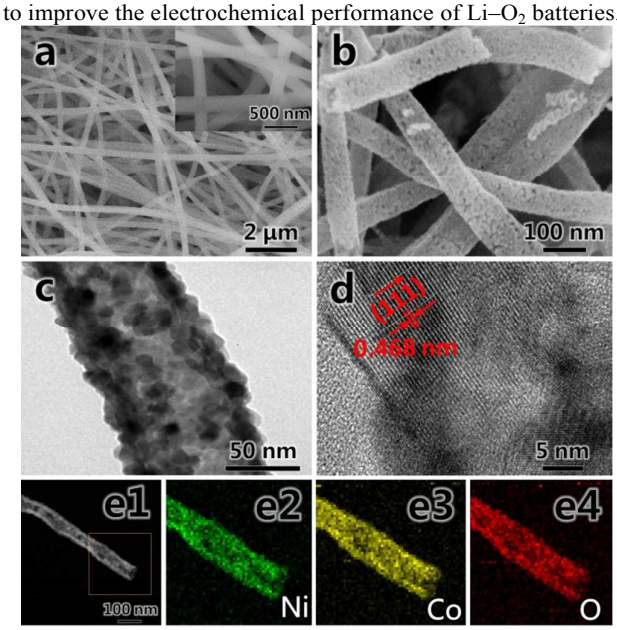

Fig. 1 FESEM (a) images at low and high (inset) magnifications for $NiCo_2O_4$ precursor nanofibers; FESEM (b), TEM (c) and HRTEM (d) images of porous $NiCo_2O_4$ nanotubes; (e1–e4) Elemental mappings show the uniformly distributed Ni, Co, and O elements in porous $NiCo_2O_4$ nanotubes.

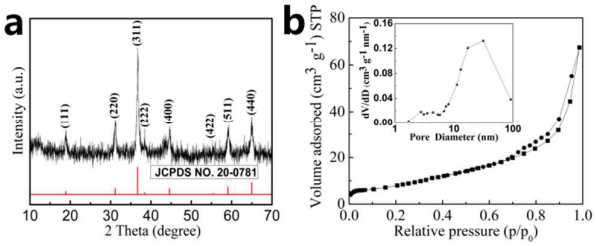

Fig. 2 (a) XRD pattern and (b) N_2 adsorption–desorption isotherms and the corresponding pore size distribution (inset) of the porous $NiCo_2O_4$ nanotubes.

The electrocatalytic activity of NCO catalyst is investigated by cyclic voltammetry (CV) at a scan rate of 0.1 mV s^{-1} (Fig. 3a). Compared with the pure acetylene carbon black (denoted as CB) cathode, NCO/CB cathode exhibits a much larger cathodic and anodic current density and a higher cathodic peak voltage, demonstrating higher bifunctional electrocatalytic activities than the CB towards ORR and OER processes in nonaqueous Li–O_2 batteries. These results illustrate that the porous NCO nanotubes would consequently exhibit remarkable electrochemical performance towards both formation and decomposition of discharge products. The electrocatalytic performance of NCO catalyst is further studied through galvanostatic charge–discharge voltage profiles. Fig. 3b shows the first full discharged–charged profiles for the Li–O_2 battery with CB and NCO/CB electrodes at a current density of 100 mA g_c^{-1}. The potential cut-off values are at 2.0 and 4.5 V for discharge and charge processes, respectively. Notably, the discharge and especially the charge cell voltage platforms can be significantly improved with the help of the NCO catalyst. In detail, the discharge voltage platform of Li–O_2 batteries with a NCO/CB electrode is about 2.63 V, which is higher than that of CB electrode by about 10–30 mV. More importantly, the charge voltage voltage of Li–O_2 batteries with NCO/CB is found to be much lower than that of CB (about 200 mV). As a result, this improvement would enhance the round-trip efficiency of the Li–O_2 battery. Remarkably, the Li–O_2 battery with NCO/CB electrode deliveres a discharge specific capacity of 5842 mAh g_c^{-1} and a charge capacity of 6022 mAh g_c^{-1} at a current density of 100 mA g_c^{-1}, which is much higher than the CB electrode at the same current density, attributing to 1D hollow mesoporous structure can effectively facilitate the electron transfer, the diffusion of electrolyte and O_2, while simultaneously supply a large contact area of electrode–electrolyte to enhance specific capacity of Li–O_2 battery. These results indicate that the NCO has a high catalytic activity toward both OER and ORR processes. The rate capability of the Li–O_2 cells with NCO/CB and CB electrodes were also examined at different current densities, as shown in Fig. 3c and d. At the current densities of 100, 200, and 500 mAh g_c^{-1}, the NCO/CB electrode is able to deliver discharge capacities of 5842, 4548, and 3105 mAh g_c^{-1}, respectively. In comparison, the CB electrode delivers decreased discharge capacities of 3234, 1880, and 979 mAh g_c^{-1}, respectively. Although the overpotential increases or discharge capacity decreases with the

current density increases, the NCO/CB electrode exhibits a higher discharge capacity and improved rate capability than those of the electrode with alone CB.

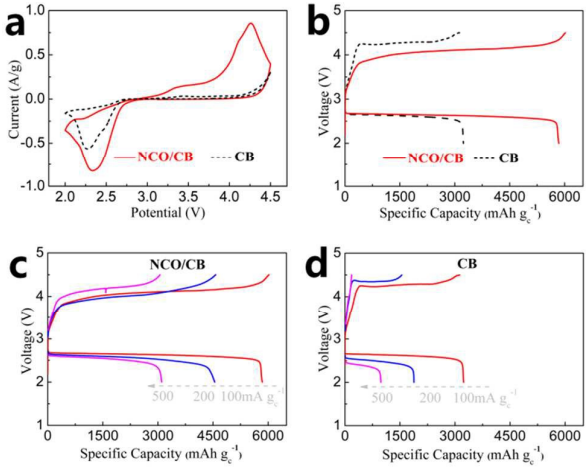

Fig. 3 (a) CV curves between 2.0 and 4.5 V at 0.1 mV s^{-1}. (b) First charge-discharge with CB and NCO/CB electrodes at a current density of 100 mA g_c^{-1} for Li–O_2 batteries in 1M LiTFSI-TEGDME electrolyte. The rate capability of NCO/CB (c) and CB (d) electrodes at various current densities.

Another considerable improvement of the Li–O_2 battery with NCO/CB electrode is the cycling stability performance. Fig. 4a–b show the cycling performance of Li–O_2 batteries fabricated with NCO/CB and CB electrodes. When testing at a current density of 200 mA g_c^{-1} with a limited capacity of 1000 mAh g_c^{-1}, the batteries with the CB electrode just exhibit 23 cycles. In contrast, the Li–O_2 battery using NCO/CB as the cathode demonstrates excellent performance over 110 cycles with the terminal discharged voltage platform of 2.4 V, and no significant changes in the discharge–charge profiles during cycling. In addition, the cycled number of NCO/CB electrode dependent discharged and charged voltage platform (half-capacity voltage) shown in Fig. 4c also reflected unconspicuous polarization during continuously performances. However, the CB electrode shows clearly decrease (in discharge) or increase (in charge) voltage platform. These results further prove the superior catalytic property of the porous NCO nanotubes for Li–O_2 battery.

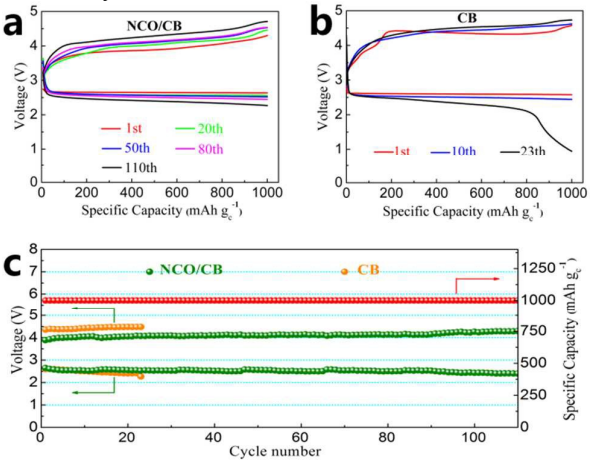

Fig. 4 Discharge–charge curves of the Li–O_2 batteries with NCO/CB (a) and CB (b) electrodes at different cycles with a limited capacity of 1000 mAh g_c^{-1} at 200 mA g_c^{-1}. (c) The cycled number dependent half-capacity voltage of the NCO/CB and CB electrodes with a limited capacity of 1000 mAh g_c^{-1} at 200 mA g_c^{-1}.

To further understand the enhanced electrochemical performances of the porous NCO nanotubes catalyst in the Li–O_2 battery, the morphologies change of the CB and NCO/CB electrodes at different discharge–recharge stages were investigated by FESEM. It can be observed from Fig. 5a that the CB electrode is composed of densely agglomerated CB nanoparticles, whereas that the NCO/CB electrode is formed by hierarchically porous composite structure with the porous NCO nanotubes catalyst and CB nanoparticles (Fig. 5b), which could provide sufficient void spaces for efficiently catalyze O_2/Li_2O_2 conversion during cycling. Fig. 5c, d show the morphologies of the discharged CB and NCO/CB electrodes at the same current density of 100 mA g_c^{-1}, respectively. The discharge products of the CB and NCO/CB electrodes are all the characteristic toroidal-shaped particles (Fig. 5c, Fig. 5d and Fig. S2), which are consistent with the previous reports of the morphology of Li_2O_2.[46–48] Interestingly, it is obvious that the size of discharge products on the NCO/CB electrode is much smaller and the discharged NCO/CB electrode also exposes many porous channels. After the subsequent recharge, most of the aggregates still remain in CB electrode (Fig. 5e), which indicates the reversibility of the CB electrode is very poor. However, the toroidal-shaped discharge products completely disappeared in the NCO/CB electrode, meanwhile the whole NCO/CB electrode with the hierarchically porous composite structure almost fully recovered, as shown in Fig. 5f. Therefore, the excellent reversibility of the NCO/CB electrode might be attributed to the high-effective bifunctional porous NCO nanotubes catalyst toward ORR and OER, leading to the much smaller size of discharge products and possessing numerously porous channels on the discharged NCO/CB electrode, which provides sufficiently product-electrolyte contact areas and thus facilitates discharge products conversion.

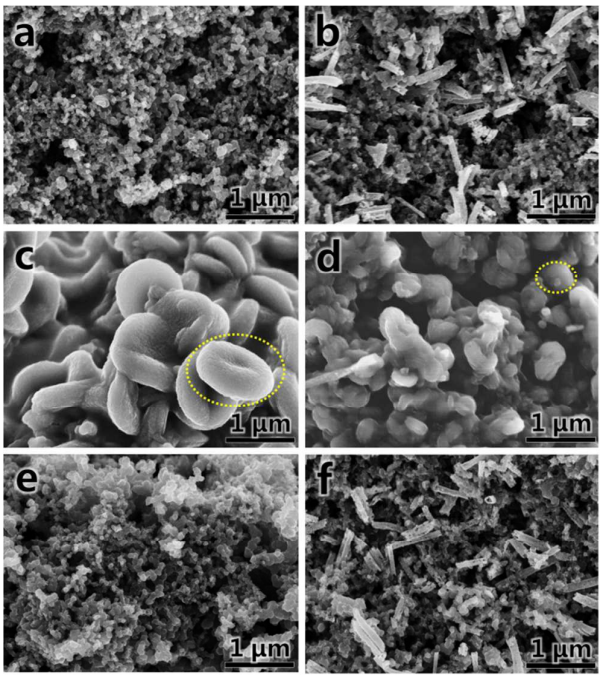

Fig. 5 FESEM images of the pristine (a, b), discharged (c, d), and recharged (e, f) CB and NCO/CB electrodes, respectively.

The excellent reversibility of NCO/CB electrode was further examined by the XRD patterns and Raman spectra analysis. The dominant discharge product is identified to be the crystalline Li_2O_2 in XRD patterns of the discharged NCO/CB electrode (Fig. 6a). After recharge, the peaks corresponding to the discharge product Li_2O_2 can be completely disappeared in XRD patterns of the recharged NCO/CB electrode. However, as the XRD patterns of CB electrode shown in Fig. S3, the peaks of the discharge product Li_2O_2 can not be full disappeared in the recharged CB electrode, which is also in agreement with the above obtained FESEM result (Fig. 5e). Furthermore, the Raman spectra indicate (Fig. 6b) that the peaks of Li_2O_2 could be clearly vanished in the recharged NCO/CB electrode. Therefore, the NCO/CB electrode shows excellent reversiblity during the discharge and charge processes. Simultaneously, the galvanostatic intermittent titration technique (GITT) is an electrochemical method that includes transient and steady-state processes, which can be utilized to determine the equilibrium voltage and overpotential in the Li–O_2 batteries.[49] The GITT result (Fig. 6c) done at 100 mA g_c^{-1} for 3h relaxation that the discharged equilibrium potential of the Li–O_2 battery is approximate to 2.9 V, which approaches the theoretical potential of Li_2O_2 formation, indicating that the generating of the discharge product Li_2O_2.[1, 50, 51] Besides, this result compares well with the XRD pattern and Raman spectrum analyses.

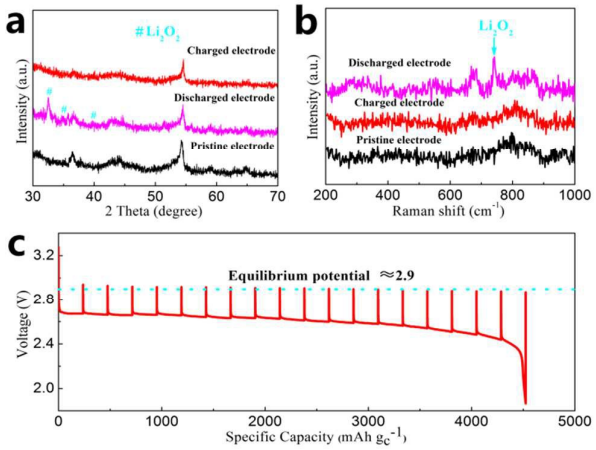

Fig. 6. XRD patterns (a) and Raman spectra (b) of the NCO/CB electrode at different discharge/charge states. (c) GITT discharge voltage profile of the NCO/CB electrode, with a relaxation time of three hours.

Conclusions

In summary, we have successfully synthesized the porous $NiCo_2O_4$ nanotubes noble metal-free catalysts by a facile and cost-effective electrospinning route for rechargeable Li–O_2 batteries. The 1D porous NCO nanotubes facilitate effectively the electron mobility, the electrolyte accessibility and the oxygen diffusion, while simultaneously provide a large contact area of electrode-electrolyte to enhance the OER and ORR reaction kinetics in Li–O_2 batteries. The as-synthesized $NiCo_2O_4$ nanotubes with hollow interior and porous wall are found to largely improve the electrochemical performance of the Li−O_2 batteries, including a high initial discharge capacity, reduced overpotential and better rate capability. Excellent cycling stability performance over 110 cycles was also achieved under with the discharged voltage platform of 2.4 V at 200 mA g_c^{-1}. From the FESEM, XRD, Raman spectroscopy and GITT analysis, toroidal-shaped Li_2O_2 particles were identified as the dominant discharge product and revealed the Li_2O_2 can be completely decomposed during the charge process, indicating its superior reversibility as effective bifunctional catalysts for Li−O_2 batteries. Therefore, this study may pave a feasible way to develop high-effective and noble metal-free catalysts for rechargeable Li–O_2 batteries.

Acknowledgements

This work was supported by the National Basic Research Program of China (973 Program) (No. 2014CB239701), National Natural Science Foundation of China (No. 21173120, No. 51372116), Natural Science Foundation of Jiangsu Province (BK2011030). This work was also supported by Funding of Jiangsu Innovation Program for Graduate Education (SJZZ15_0042, KYLX_0254), the Fundamental Research Funds for the Central Universities, a Funding for Outstanding Doctoral Dissertation in NUAA (BCXJ14-12) and a Project

Funded by the Priority Academic Program Development of Jiangsu Higher Education Institutions (PAPD).

Notes and references

1. K. M. Abraham and Z. Jiang, *J. Electrochem. Soc.*, 1996, **143**, 1–5.
2. P. G. Bruce, S. A. Freunberger, L. J. Hardwick and J. M. Tarascon, *Nat. Mater.*, 2012, **11**, 19–29.
3. R. Black, B. Adams and L. F. Nazar, *Adv. Energy Mater.*, 2012, **2**, 801–815.
4. Y. Chen, S. A. Freunberger, Z. Peng, O. Fontaine and P. G. Bruce, *Nat. Chem.*, 2013, **5**, 489–494.
5. Z. Y. Guo, D. D. Zhou, X. L. Dong, Z. J. Qiu, Y. G. Wang and Y. Y. Xia, *Adv. Mater.*, 2013, **25**, 5668–5672.
6. Z. L. Jian, P. Liu, F. J. Li, P. He, X. W. Guo, M. W. Chen and H. S. Zhou, *Angew. Chem. Int. Ed.*, 2014, **53**, 442–446.
7. H.-G. Jung, J. Hassoun, J.-B. Park, Y.-K. Sun and B. Scrosati, *Nat. Chem.*, 2012, **4**, 579–585.
8. J. J. Xu, Z. L. Wang, D. Xu, L. L. Zhang and X. B. Zhang, *Nat. Commun.*, 2013, **4**, 2438.
9. X. F. Hu, F. Y. Cheng, X. P. Han, T. R. Zhang, J. Chen, *Small*, 2014, **11**, 809-813.
10. Z. Y. Guo, G. N. Zhu, Z. Qiu, Y. G. Wang and Y. Y. Xia, *Electrochem. Commun.*, 2012, **25**, 26–29.
11. F. J. Li, D. M. Tang, Y. Chen, D. Golberg, H. Kitaura, T. Zhang, A. Yamada and H. S. Zhou, *Nano Lett.*, 2013, **13**, 4702–4707.
12. X. F. Hu, X. P. Han, Y. X. Hu, F. Y. Cheng and J. Chen, *Nanoscale*, 2014, **6**, 3522–3525.
13. W.J. Kwak, K. C. Lau, C.D. Shin, K. Amine, L. A. Curtiss and Y.-K. Sun, *ACS Nano*, 2015, **9**, 4129–4137.
14. M. Prabu, K. Ketpang and S. Shanmugam, *Nanoscale*, 2014, **6**, 3173–3181.
15. Z. Peng, S. A. Freunberger, Y. Chen and P. G. Bruce, *Science*, 2012, **337**, 563–566.
16. H.D. Lim, H. Song, H. Gwon, K.Y. Park, J. Kim, Y. Bae, H. Kim, S.K. Jung, T. Kim, Y. H. Kim, X. Lepro, R. Ovalle-Robles, R. H. Baughman and K. Kang, *Energy Environ. Sci.*, 2013, **6**, 3570–3575.
17. E. Yilmaz, C. Yogi, K. Yamanaka, T. Ohta and H. R. Byon, *Nano Lett.*, 2013, **13**, 4679–4684.
18. D. W. Su, S. X. Dou and G. X. Wang, *J. Mater. Chem.*, 2015, **3**, 18384–18388.
19. M. M. Ottakam Thotiyl, S. A. Freunberger, Z. Peng and P. G. Bruce, *J. Am. Chem. Soc.*, 2013, **135**, 494–500.
20. B. D. McCloskey, A. Speidel, R. Scheffler, D. C. Miller, V. Viswanathan, J. S. Hummelshøj, J. K. Nørskov and A. C. Luntz, *J. Phys. Chem. Lett.*, 2012, **3**, 997–1001.
21. F. J. Li, D. M. Tang, Z. L. Jian, D. Liu, D. Golberg, A. Yamada and H. S. Zhou, *Adv. Mater.*, 2014, **26**, 4659–4664.
22. B. D. McCloskey, R. Scheffler, A. Speidel, D. S. Bethune, R. M. Shelby and A. C. Luntz, *J. Am. Chem. Soc.*, 2011, **133**, 18038–18041.
23. D. M. Itkis, D. A. Semenenko, E. Y. Kataev, A. I. Belova, V. S. Neudachina, A. P. Sirotina, M. Hävecker, D. Teschner, A. Knop-Gericke, P. Dudin, A. Barinov, E. A. Goodilin, Y. Shao-Horn and L. V. Yashina, *Nano Lett.*, 2013, **13**, 4697–4701.
24. Z. Y. Guo, D. D. Zhou, H. J. Liu, X. L. Dong, Y. S. Yi, A. S. Yu, Y. G. Wang and Y. Y. Xia, *J. Power Sources*, 2015, **192**, 181–188.
25. A. Debart, A. J. Paterson, J. Bao and P. G. Bruce, *Angew. Chem. Int. Ed.*, 2008, **47**, 4521–4524.
26. W.H. Ryu, T.H. Yoon, S. H. Song, S. Jeon, Y.J. Park and I.D. Kim, *Nano Lett.*, 2013, **13**, 4190–4197.
27. W. Yang, J. Salim, C. Ma, Z. Ma, C. Sun, J. Li, L. Chen and Y. Kim, *Electrochem. Commun.*, 2013, **28**, 13–16.
28. Q. Li, P. Xu, B. Zhang, H. Tsai, J. Wang, H. L. Wang and G. Wu, *Chem. Commun.*, 2013, **49**, 10838–10840.
29. J. Lu, Y. Qin, P. Du, X. Luo, T. Wu, Y. Ren, J. Wen, D. J. Miller, J. T. Miller and K. Amine, *RSC Adv.*, 2013, **3**, 8276–8285.
30. M. Prabu, P. Ramakrishnan and S. Shanmugam, *Electrochem. Commun.*, 2014, **41**, 59–63.
31. M. Prabu, P. Ramakrishnan, H. Nara, T. Momma, T. Osaka and S. Shanmugam, *ACS Appl.Mater.Interfaces*, 2014, **6**, 16545–16555.
32. R. Black, J.-H. Lee, B. Adams, C. A. Mims and L. F. Nazar, *Angew. Chem. Int. Ed.*, 2013, **125**, 410–414.
33. Q.C. Liu, J.J. Xu, Z.W. Chang and X.B. Zhang, *J. Mater. Chem.*, 2014, **2**, 6081–6085.
34. L. F. Shen, Q. Che, H. S. Li, X. G. Zhang, *Adv. Funct. Mater.*, 2014, **24**, 2630–2637.
35. G. Zhang and X. W. Lou, *Adv. Mater.*, 2013, **25**, 976–979.
36. T.Y. Wei, C.H. Chen, H.C. Chien, S.Y. Lu and C.C. Hu, *Adv. Mater.*, 2010, **22**, 347–351.
37. L. Shen, L. Yu, X.-Y. Yu, X. Zhang and X. W. Lou, *Angew. Chem. Int. Ed.*, 2015, **54**, 1868–1872.
38. L. Zhang, S. Zhang, K. Zhang, G. Xu, X. He, S. Dong, Z. Liu, C. Huang, L. Gu and G. Cui, *Chem. Commun.*, 2013, **49**, 3540–3542.
39. B. Sun, X. Huang, S. Chen, Y. Zhao, J. Zhang, P. Munroe and G. X. Wang, *J. Mater. Chem.*, 2014, **2**, 12053–12059.
40. B. Sun, J. Zhang, P. Munroe, H.-J. Ahn and G. X. Wang, *Electrochem. Commun.*, 2013, **31**, 88–91.
41. F. Lu, X. Cao, Y. Wang, C. Jin, M. Shen and R. Yang, *RSC Adv.*, 2014, **4**, 40373–40376.
42. S. Peng, Y. Hu, L. Li, X. Han, F. Cheng, M. Srinivasan, Q. Yan, S. Ramakrishna and J. Chen, *Nano Energy*, 2015, **13**, 718–726.
43. S. G. Mohamed, Y.Q. Tsai, C.J. Chen, Y.T. Tsai, T.F. Hung, W.S. Chang and R.S. Liu, *ACS Appl. Mater. Interfaces*, 2015, **7**, 12038–12046.
44. S. Peng, L. Li, Y. Hu, M. Srinivasan, F. Cheng, J. Chen and S. Ramakrishna, *ACS Nano*, 2015, **9**, 1945–1954.
45. L. L. Li, S. J. Peng, Y. L. Cheah, P. F. Teh, J. Wang, G. Wee, Y. W. Ko, C. L. Wong and M. Srinivasan**,** *Chem. - Eur. J.*, 2013, **19**, 5892–5898.
46. D. Kundu, R. Black, E. J. Berg and L. F. Nazar, *Energy Environ. Sci.*, 2015, **8**, 1292–1298.
47. J. Lu, Y. Lei, K. C. Lau, X. Luo, P. Du, J. Wen, R. S. Assary, U. Das, D. Miller, J. W. Elam, H. M. Albishri, D. A. El-Hady, Y. K. Sun, L. A. Curtiss and K. Amine, *Nat. Commun.*, 2013, **4**, 2255.
48. J.J. Xu, Z.L. Wang, D. Xu, F.Z. Meng and X.B. Zhang, *Energy Environ. Sci.*, 2014, **7**, 2213–2219.
49. Z. H. Cui, X. X. Guo and H. Li, *Energy Environ. Sci.*, 2015, **8**, 182–187.
50. P. G. Bruce, S. A. Freunberger, L. J. Hardwick and J. M. Tarascon, *Nat. Mater.*, 2012, **11**, 172–172.
51. H.K. Lim, H.D. Lim, K.Y. Park, D.H. Seo, H. Gwon, J. Hong, W. A. Goddard, H. Kim and K. Kang, *J. Am. Chem. Soc.*, 2013, **135**, 9733–9742.

Table of Contents

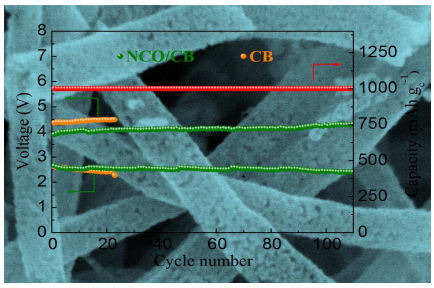

Porous $NiCo_2O_4$ nanotubes as a effective bifunctional catalyst for rechargeable Li–O_2 batteries with a excellent cycling stability.